JOURNAL OF GEOPHYSICAL RESEARCH, VOL. 102, NO. D4, PAGES 4357–4365, FEBRUARY 27, 1997

Tomography of the Earth's atmosphere by the spaceborne occultation radiometer ORA: Spatial inversion algorithm

Didier Fussen, Etienne Arijs, Fabienne Leclere, Dennis Nevejans and Christine Bingen

Belgian Institute for Space Aeronomy, Brussels, Belgium

Abstract. The occultation radiometer ORA was designed to perform measurements of O_3, NO_2 , H_2O, number density, and aerosol extinction altitude profiles in the Earth's atmosphere through the occultation method viewing the full solar disk. The experiment was mounted on the EURECA satellite and measured the relative transmission of light during about 7000 orbital sunsets and sunrises from August 11, 1992, to May 13, 1993. The spatial inversion algorithm developed to retrieve the total extinction altitude profiles from these data is described here. It is shown that the signal measured by an instrument having a large field of view can be successfully processed to give a much better altitude resolution than the one related to the angular size of the Sun. The main difficulties concern the inclusion of all refractive effects, the application of a new inversion scheme and its associated mapping strategy to refine the aerosol layer detection. The algorithm applies to fully nonlinear occultation experiments requiring global and nonheuristic inversion schemes.

1. Introduction

In recent years, diverse remote sensing methods, e.g., SAGE [*Mauldin et al.*, 1985], HALOE [*Russell et al.*, 1993], CLAES [*Roche et al.*, 1993], have been developed for the measurement of minor constituent and aerosol vertical profiles in the Earth's atmosphere from spaceborne instruments. One approach, the occultation technique or limb tomography [*Roble and Hays*, 1972], relies upon measurement of the relative transmission of the light emitted by an extraterrestrial source (usually the Sun) through the atmosphere as the satellite enters or leaves the Earth's shadow along its orbit (see Figure 1). Besides the possibility of working with high spectral selectivity, the method has a fundamental advantage: it is self-calibrating, i.e., the the information is extracted from the relative intensity with respect to the unattenuated intensity.

The European Retrievable Carrier (EURECA) satellite was launched by the European Space Agency (ESA) in July 1992 for a 1-year mission. For this mission, the Belgian Institute for Space Aeronomy developed a simple UV-visible radiometer (named ORA for "Occultation RAdiometer") for the purpose of measuring O_3, NO_2, H_2O and aerosol extinction altitude profiles. It was accompanied by an infrared radiometer designed by the Department for Atmospheric, Oceanic and Planetary Physics of the University of Oxford to measure upper atmospheric water vapor [*Calcutt et al.*, 1993].

The ORA instrument has been described elsewhere [*Arijs et al.*, 1995]. Briefly, it consists of eight independent radiometers of similar design, each containing a quartz window, an interference filter, and a simple optics followed by a photodiode detector. The nominal operating wavelength of the modules and the related atmospheric major constituents are summarized in Table 1. From August 1992 to May 1993 the instrument measured about 7000 sunrises and sunsets from its quasi-circular orbit at an altitude of 508 km.

The low-orbit inclination of the satellite (28°) limited the latitude coverage between 40°S and 40°N. Owing to the minimal acceleration level requirements of the carrier, mainly dedicated to microgravity studies, and to the power and weight constraints , no Sun-pointing or scanning system coupled with a telescope was integrated to the ORA instrument. Instead, its line of sight was aligned with the optical axis of the Sun-tracking system of the satellite, which had a pointing accuracy of only 1°. Therefore, to guarantee a full view of the solar disk, a ±2° optical field of view for the ORA modules was chosen. This means that the angular extension of the sampled atmospheric region during the occultation was defined by the apparent angular size of the Sun itself (about 0.5°, representing 25 km along the vertical direction).

Paper number 96JD03001
0148-0227/97/96JD-03001$09 00

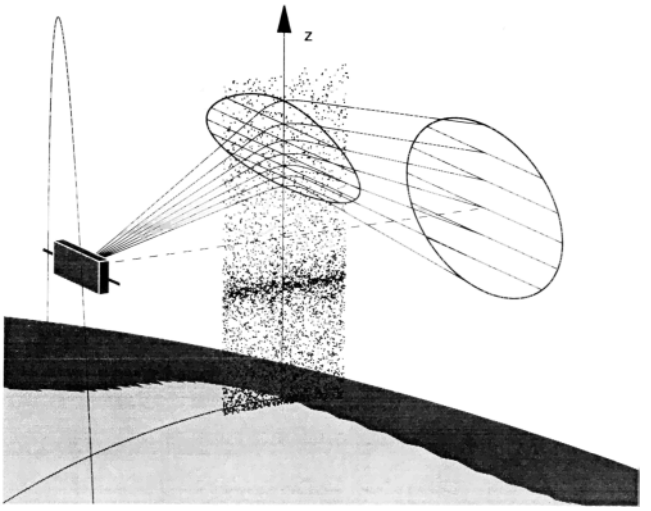

Figure 1. Simplified view of the occultation geometry for the ORA experiment. Without atmosphere, a central ray (dashed line) would graze the Earth's surface at a lower altitude than the true refracted ray. Note that rays emitted from the top of the Sun are less refracted than those emitted from the bottom, resulting in an inhomogeneous Sun flattening.

Any occultation experiment has to face the so-called inverse problem of retrieving the attenuation altitude profile that gave rise to the measured signal. In particular, ORA had a low spatial resolution, theoretically compensated, however, by a very large signal to noise ratio. This peculiar situation made it a challenge to construct a fast and robust algorithm capable of reconstructing the number density altitude profiles. The inverse problem can be divided into two parts. The spatial inversion concerns the retrieval of the total extinction coefficient as a function of altitude from the measured signals. On the other hand, the spectral inversion deals with the retrieval of the constituent number densities, at each altitude, using the total extinction coefficients in all channels simultaneously.

The purpose of this paper is to outline the different problems encountered in the data reduction and to explain the principles of the new spatial inversion method we developed to this end. As is explained below the spectral inversion scheme will be described in a forthcoming paper.

2. Formulation of the Signal

At any moment during the occultation and for a weakly refracting atmosphere there exists a one-to-one relation between the time and the trajectory of a ray issued from a particular point on the Sun and passing above the Earth's surface at an altitude h. In the single scattering regime and for monochromatic radiation at wavelength λ the transmitted relative intensity through the atmosphere is

$$T_\lambda(h) = \exp\left(-\int_{s_1}^{s_2} \beta_\lambda\{z[s(h)]\}\, ds\right) \qquad (1)$$

where s is the length element along the optical path crossing the atmosphere and β_λ is the total attenuation coefficient which is supposed to be only a function of the local altitude z. This coefficient can be decomposed in contributions of different scatterers or absorbers, depending on the channel nominal wavelength:

$$\beta_\lambda = \beta_\lambda^{\text{Rayleigh}} + \beta_\lambda^{\text{Aerosol}} + \beta_\lambda^{O_3} + \ldots \qquad (2)$$

where the superscript "Rayleigh" refers to the molecular light scattering by the air.

Considering that the instrument collects rays coming from the whole solar disk, we obtain for the total relative signal at wavelength λ

$$S_\lambda(h) = \int_{\Delta\Omega} W(\Omega)\, T_\lambda[h(\Omega)]\, d\Omega \qquad (3)$$

Here $\Delta\Omega$ represents the solid angle domain spanned by the apparent Sun, while $W(\Omega)$ expresses the relative light distribution across the solar disk. The total measured signal is finally obtained through integration over the wavelength bandwidth of the filter to include filter characteristics and detector sensitivity as well as the solar spectral distribution:

$$S(h) = \frac{\int_{\Delta\lambda} S_\lambda(h)\, d\lambda}{\Delta\lambda} \qquad (4)$$

There is a simple relation between the attenuation coefficient for a particular constituent X at wavelength λ and the number density $n^{[X]}$ of this constituent:

$$\beta_\lambda^{[X]}(z) = \sigma_\lambda\, n^{[X]}(z) \qquad (5)$$

where σ_λ is the effective total cross section for the considered attenuation process. It is very important to note that the latter relation is not true for aerosols, for which it is well known that the particle size distribution is broad. The aerosol scattering cross section which is clearly dependent on the particle typical size r (for a given shape and chemical composition) can be written as

$$\beta_\lambda^{\text{Aerosol}} = \int_0^\infty \sigma_\lambda(r)\, \frac{dn^{\text{Aerosol}}}{dr}\, dr \qquad (6)$$

where dn^{Aerosol}/dr stands for the aerosol size function.

Table 1. Major Light Absorbers at the Different UV-Visible Channels

λ, nm	Predominant Constituent
259	O_3, air
340	air, aerosols
385	aerosols, NO_2
435	aerosols, NO_2
442	aerosols, NO_2
600	O_3, aerosols
943	H_2O, aerosols
1013	aerosols

It should be well understood that occultation experiments only give access to β while any aerosol number density derivation presupposes both an optical model (like Mie scattering) and the knowledge of the particle size distribution.

3. Optical Computations

3.1. Ray Tracing

From equation (1) it is evident that the first task of the retrieval procedure was to compute the optical path associated with all detected solar rays. This is a simple job only for grazing heights above 40 km, where refraction by the Earth's atmosphere becomes negligible. Starting from astronomical ephemerides and the measured satellite state vector in a geocentric reference frame, the geometrical grazing height g (i.e., defined by the straight line joining the Sun and the detector) is computed by considering the Earth as a standard ellipsoid. At the grazing point the surface of the Earth is approximated by a sphere tangent to the ellipsoid with the same curvature.

It is clear that the gradient of refraction index (proportional to air density) is much more important along the local vertical than along any orthogonal direction. It is a good approximation to consider that the refraction index $N(R)$ has only a radial dependence and that the light trajectory lies in the refraction plane containing the emitter Sun point, the center of the approximating sphere and the satellite. The ray path obeys the following differential equation [*Born and Wolf*, 1993]

$$\frac{dR}{d\theta} = \pm\frac{R}{K}\cdot\sqrt{N^2(R)\,R^2 - K^2} \tag{7}$$

where θ is the polar angle in the refraction plane and the turning point is defined by $dR/d\theta = 0$. Bouguer's law expresses the momentum conservation as

$$K = \| \vec{R} \times N \vec{S} \| = \text{const} \tag{8}$$

where $\vec{S}$ is the unitary vector tangent to the trajectory. Consequently, the angle defining the penetration of a ray in the atmosphere determines the value of K, which in turn, determines the grazing altitude.

We recognize here a boundary value problem because the position of the satellite is known but not the angle under which the ray enters the instrument. Therefore the full problem has been solved iteratively by a shooting method using a classical Runge-Kutta scheme with variable step size to integrate (7) [*Press et al.*, 1992].

The solution trajectory was recorded as an array of optical segments. It has been chosen to divide the Sun disk into horizontal slices to represent its angular extension, assuming that refraction acts uniformly in the orthogonal direction to the refraction plane. A division of 20 slices was found to give a sufficient accuracy in the angular integration (see 3).

The whole procedure was repeated for about 100 orbit positions occupied during the occultation and produced a 2 M-byte optical segment file to be passed to the spatial inversion module. In view of the high computation cost and the quite large angular extension of the Sun, we decided to neglect both the chromatic refraction effects and the actual atmosphere status along the trajectory. The refractivity altitude profile was computed with Edlen's formula [*Edlen*, 1953] using a mean wavelength of 600 nm and the U.S. Standard Atmosphere (1976). Numerical verifications have shown that the error introduced on grazing altitudes was less than 1 km. This should be taken into account when evaluating the final accuracy of the retrieved altitude profiles.

When dividing the Sun into slices, we must take into account the nonuniform contributions of the slices across the solar disk. The first effect is, of course, the relative surface of each slice. The second effect is the solar limb darkening that has been integrated for each wavelength [*Allen*, 1985], [J. Sauval, private communication, 1994].

3.2. Refractive Effects

Refraction in the atmosphere actually produces several effects in an occultation experiment. Refraction not only increases the true grazing height h up to 14 km (for a tangent geometrical path), but it also bends the rays (up to 1° i.e., twice the Sun's diameter), shifting the occultation time period (up to 20 s) before geometrical sunrise or after geometrical sunset. Furthermore, the optical path length is increased in the absorbing medium.

The atmosphere can be viewed as a kind of diverging lens [*Garriott*, 1979] where the bending of the rays increases (however, not linearly) as they get closer to the surface. The image of the Sun through the atmosphere is consequently affected by refraction because rays coming from the "bottom" are more refracted than those coming from the "top", which results in Sun flattening (typical values are 15% at 30 km, 38% at 20 km, and 69% at 10 km). Sun flattening is also associated with a less intuitive phenomenon: the refractive dilution effect.

We want to give here an approximate description of the latter effect, assuming an infinitely thin atmosphere (in the refraction plane). This is a reasonable assumption in view of the distance between the satellite and the grazing point ($\sim$2500 km) and also because of the exponential decay of the air density with a 7-km scale height. This is equivalent to recognizing that most of the refraction occurs in a narrow region around the grazing point. For the sake of simplicity, we also consider a unidimensional Sun (see Figure 2). A ray emitted from the Sun point Y can be represented by a straight line having a slope M until it crosses the atmosphere at $x = 0$, where refraction takes place. The refracted ray reaches the satellite with a different slope m, given by

$$m(z) = M(z) + \Delta m(z) \tag{9}$$

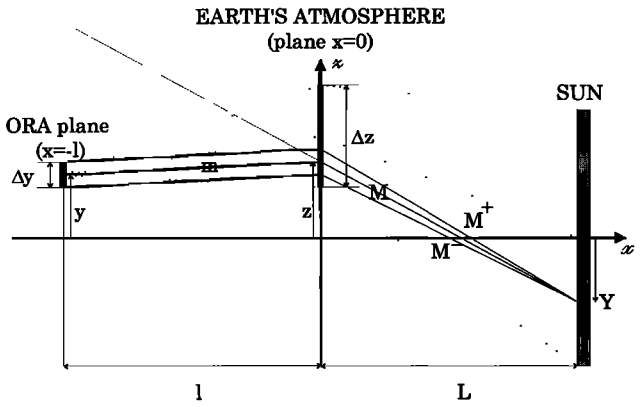

Figure 2. Unidimensional model for refractive dilution. Rays are emitted from the Sun at $x = L$, while refraction is assumed to occur at the grazing point $x = 0$. Trajectories are bent with a slope change depending on the local altitude z. The ray pencils hit the satellite plane at $x = -l$

where z is the altitude of the crossing. Considering the Sun-Earth and Earth-satellite distances (L and l, respectively), we have

$$M = \frac{Y - z}{L} \tag{10}$$

$$m = \frac{z - y}{l} \tag{11}$$

$$(L + l)\, z = L\, y + l\, Y + L\, l\, \Delta m(z) \tag{12}$$

The energy flux Φ hitting a plane containing the satellite and orthogonal to the refraction plane is equal to the sum of the fluxes contained in all pencils of rays emitted from the Sun and reaching an infinitesimal length element Δy centered on y. If M^+ and M^- are the slopes of the extreme rays falling on Δy for the pencil emitted from Y and if $| M | \ll 1$, the energy flux contained in this pencil is clearly proportional to $(M^+ - M^-)$, and the total flux is

$$\begin{aligned} \Phi &= \lim_{\Delta y \to 0} \left| C \int_{Y_1}^{Y_2} \frac{(M^+ - M^-)}{\Delta y}\, dY \right| \\ &= \left| C \int_{Y_1}^{Y_2} \frac{\partial M}{\partial y|_Y}\, dY \right| \end{aligned} \tag{13}$$

where C is an appropriate constant factor and the bounds Y_1 and Y_2 define the solar disk. Keeping Y fixed for awhile, we have

$$\frac{\partial M}{\partial y|_Y} = \frac{-1}{L} \frac{\partial z}{\partial y|_Y} \tag{14}$$

where y is the satellite position on a screen where we want to evaluate the solar flux. On the other hand, it follows from (12) that

$$\frac{\partial z}{\partial y|_Y} = \frac{L}{l + L} + \frac{l\, L}{l + L} \frac{d\Delta m(z)}{dz} \frac{\partial z}{\partial y|_Y} \tag{15}$$

leading to

$$\Phi = \left| C \int_{Y_1}^{Y_2} \frac{dY}{L + l - L\, l \frac{d\Delta m(z)}{dz}} \right| \tag{16}$$

When Y is varying and y is constant, the total differential of (12) is

$$(L + l)\, dz = l\, dY + L\, l\, d[\Delta m(z)] \tag{17}$$

Combining now equations (16) and (17), we get for Φ,

$$\Phi = \left| \frac{C}{l} \int_{Y_1}^{Y_2} \frac{1}{\frac{dY}{dz}}\, dY \right| = \left| \frac{C}{l} \Delta z \right| \tag{18}$$

This means that the energy flux reaching the detector will be proportional to the apparent size of the source for the above-mentioned hypothesis. The effect is far from being negligible, in view of the importance of the Sun flattening, and we have corrected the transmission signal for each Sun slice.

4. Spatial Inversion Problem

Inspection of equations (1)-(4) shows that it is not possible to directly separate the different extinction coefficients as expressed by equation (2) by taking the logarithm of the relative transmission to get the optical thickness. This is only allowed for instruments having a field of view much smaller than the Sun angular size and for which the $W(\Omega)$ function looks like a Dirac delta function. This is a real problem because different constituents have different contributions at separate wavelengths, as for instance, air density or aerosol. Furthermore, the relative importance of these contributions may vary with altitude. It would hence be unrealistic to develop, in the case of ORA, an algorithm capable of retrieving the altitude extinction profiles ("spatial inversion") and simultaneously the associated constituents ("spectral inversion") .

Accordingly we decided to perform the spatial inversion first, as it is described in this paper, being aware that high inversion residuals could impair spectral inversion for minor constituents. On the other hand, this dichotomy makes the spatial resolution analysis easier, while the full spectral inversion algorithm can be tackled independently afterward.

Because of the nonlinearity of the spatial inversion and the consequent use of iterative methods until convergence, the globality of the obtained solution should always be investigated. This means that the robustness of the algorithm has to be checked against the first-guess profile choice and the influence of outlying data points. As a systematic, although vague, criterion, we always required the solution to be not too far from expected. This somewhat arbitrary choice is nothing more than the use of a priori information that is unavoidable in solving this kind of problem, for which there are no theorems about the number of solutions.

A completely independent question concerns the large overlap between two consecutive measurements on the orbit (typical by $\Delta h \simeq 1$ km) due to the large field of view of the instrument. This causes a systematic ill-conditioning (in linear or nonlinear problems) because each measurement is close to the preceding one and can only bring new information if the signal to noise ratio is high. Indeed, the angular integration smooths the altitude profile structures out, but the signal gets higher so that its derivatives may contain signatures of these structures. The true spatial resolution of ORA for the total attenuation profile is therefore determined not only by the field of view (poor), but also by the signal to noise ratio (good, because the whole solar disk is seen) and also by the profile morphology itself (smooth for air, sharp for aerosol or ozone).

In a recent work [*Fussen*, 1995], we described the inadequacy of well-known heuristic methods to solve inverse problems with a large field of view. Onion peeling or Chahine algorithms [*Chahine*, 1972] suffer all of the drawbacks of adjusting the current solution locally (layer per layer) in an iterative way. They turned out to be unstable or inaccurate in the present case and they do not answer the question of solution uniqueness (see e.g. [*Rodgers*, 1976]. Sometimes they need to be stopped after an unpredictable number of iterations to prevent spurious profile oscillations from developing. In a recent paper, *Lumpe et al.* [1991] presented an elegant method to solve the problem analytically restricted, however, to a nonrefractive atmosphere.

5. The NOPE Method

The philosophy behind the natural orthogonal polynomial expansion (NOPE) method, which was described by *Fussen* [1995], is based upon three major ideas.

First, local methods have been abandoned in favor of a global one that would adjust the whole extinction profile after each iteration (and that would avoid intricate upward or downward error propagation analysis).

The second idea was to recognize that a good description of an altitude profile for, say, 50 atmospheric layers does not systematically require the determination of 50 parameters. An appropriate mathematical description using a smaller parameter set can meet the objectives for required accuracy. This was obviously an application for a basis of orthogonal polynomials so that we express the extinction profile as the series

$$\beta(z) = \beta_0(z) \sum_{i=0}^{I} \alpha_i \widetilde{P}_i(z) \tag{19}$$

The $\widetilde{P}_i(z)$ are orthonormal polynomials of the order i, the α_i are linear coefficients characterizing the solution, and $\beta_0(z)$ is any well-defined a priori solution, constructed for example, from a standard atmosphere model and the knowledge of extinction cross sections and instrument spectral function. The expansion is truncated after I terms without problems if the convergence rate is fast enough ($I = 10$ was found to be a safe value to ensure convergence). The orthonormality property is related to the scalar product

$$\int_0^\infty \widetilde{P}_i(z)\, \widetilde{P}_j(z)\, w(z)\, dz = \delta_{ij} \tag{20}$$

where $w(z)$ is the weight function [*Abramowitz and Stegun*, 1972].

The third and subtlest idea of the method was to exploit the fact that, among the infinite class of orthogonal polynomial sets defined by a $w(z)$ function, a privileged choice could be

$$w(z) = \frac{\beta_0(z)}{\int_0^\infty \beta_0(z)\, dz} \tag{21}$$

By doing so, we constrain the orthogonal polynomial family to be very sensitive to (or to be "focused" on) altitude regions where structures are expected to occur. In Figure 3 a typical total extinction altitude profile at 600 nm is shown wherein the signature of the ozone layer is reduced to a bump on a logarithmic scale. While several authors [*Twomey*, 1975] warn against arbitrary use of prior knowledge, we want to underline here that NOPE systematically uses the a priori information but in a rigorous mathematical context. The special choice of $w(z)$ is nothing more than a convergence accelerator for the expansion or a "window of interest" weighting procedure.

The final solution to the spatial inversion is finally obtained by applying a standard Levenberg-Marquardt

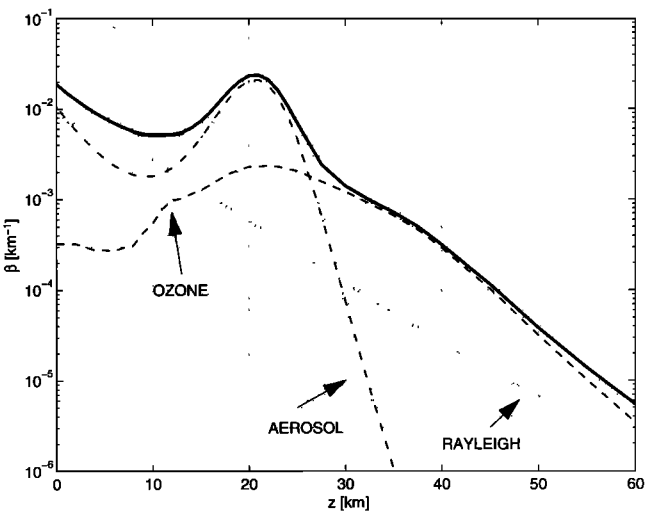

Figure 3. Typical total extinction profile (km^{-1}) versus altitude (km) at 600 nm. This profile is the sum of three contributions (molecular number density, ozone, and aerosol) acting with different magnitudes in overlapping regions. The retrieved total profile after spatial inversion has to preserve these fine details to allow successful spectral inversion.

minimization procedure [*Press et al.*, 1992] to the merit function

$$\chi^2 = \sum_{k=1}^{k_m} [s_k - S_\lambda(h_k; \{\alpha_0, \alpha_1, \ldots \alpha_I\})]^2 \qquad (22)$$

where s_k is the measured signal for the k_m measurements during the occultation.

The following important points should be kept in mind:

1. If $\beta(z)$ was equal to $\beta_0(z)$, the solution vector would be $\overrightarrow{\alpha} = \{1, 0, \ldots 0\}$ .It is thus expected that the actual solution has a decreasing series of α_i if the actual atmosphere can be considered as a perturbed standard atmosphere. If it was very different from $\beta_0(z)$, it would be systematically detected by inspecting the expansion convergence rate. In such a case, the remedy would be simply to correct $\beta_0(z)$ in the appropriate way by using extra information or by increasing I.

2. Orthogonality assures that the information content carried by α_i is independent (and usually smaller in magnitude) than the one carried by α_{i-1}. As the number of basis functions is increased, the last terms of the expansion are just small corrections relative to the first terms which contain the largest structures.

3. The uniqueness problem is now addressed in the following way : we still don't know whether there exists a better solution (local or global) for a given inversion problem but the solution obtained by NOPE should normally be the closest one to the reasonable mean state of the atmosphere defined by $\beta_0(z)$.

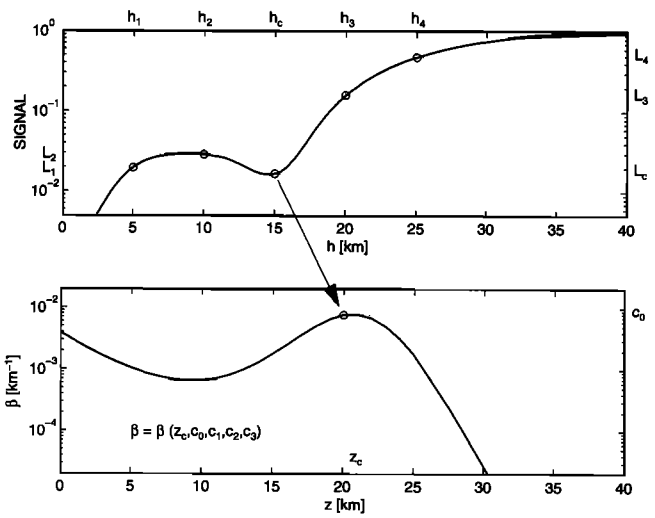

Figure 4. Illustration of the mapping strategy. The synthetic signal (top) exhibits a minimum (note the logarithmic scale) which can be clearly related to the centroid of the model profile (bottom) used to generate this signal. The objective of the mapping will be to establish a rough correspondence between selected nodes on the signal (around h_c) and the profile parameters.

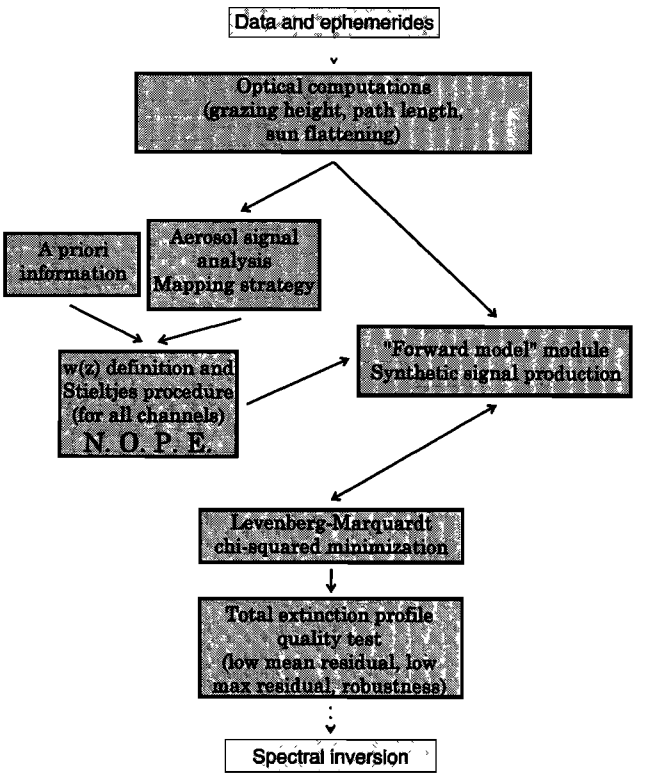

Figure 5. ORA spatial inversion flowchart. Note that the whole sequence is completely performed for each event.

6. The Inversion Procedure

For all the ORA channels we can compute $\beta_0^{[\lambda]}(z)$ and generate the adequate polynomial set using, for instance, a Stieltjes procedure [*Press et al.*, 1992]. A last difficulty subsists, however, with the aerosols, for which the information concerning the wavelength dependence of the extinction profile is scarce in the post-Pinatubo period (a much flatter curve is the only dominant aspect). Furthermore, the altitude profiles may exhibit high variabilities over short time or geographical ranges [*Brogniez and Lenoble*, 1991].

For the ORA experiment some channels (in particular at λ = 943 and 1013 nm) were dominated by the still large Pinatubo aerosol effect. This caused strong attenuation (also called signal saturation), reducing the relative importance of the aerosol layer signature on the signal. Moreover, the sharp structure of the Junge layer (about 5 km full width at half maximum) could be contaminated for a large field of view instrument by a "cut-off" attenuation due to tropospheric or stratospheric clouds [*Kent et al.*, 1993]. Therefore a simple mean exponential (monotonic) aerosol profile used to construct $\beta_0(z)$ turned out to be inadequate and produced a local solution not capable of reproducing the signal bump characteristic of the aerosol layer. To ameliorate the result at low altitudes, we adopted the following strategy.

By simply looking at the ORA signal, we can easily detect an aerosol layer signature as a bump (or a hole) in the tail of the transmitted intensity. This information should be passed to the inversion algorithm to emphasize that region. First, we have defined a more elaborate generic aerosol profile as

$$\beta_g(z) = c_0 \exp\left(-\frac{c_1\,\delta^2 + \delta^3}{c_2 + c_3\,\delta^2}\right), \delta = (z - z_c) \qquad (23)$$

where $\vec{V} = [z_c\, c_0\, c_1\, c_2\, c_3]$ is a vector of free parameters. With this analytic form, $\beta_g(z)$ may (or not as the free parameters are varied) represent a maximum at the centroid $z = z_c$ while it is always asymptotic (for high altitude) to a pure exponential behavior. The set of parameters has been varied over a large range, and about 2700 synthetic occultations have been produced as "forward" computations. The strategy consisted of an approximate mapping between the signal and the parameter set (see Figure 4). The synthetic signal can be numerically analyzed, and an extremum (in the curve or in its derivatives) is detected at $h = h_c$. Four symmetrical adjacent nodes are defined at h_1,h_2,h_3,h_4, together with the logarithm of the transmission, L_1,L_2,L_3,L_4, respectively . Let us define the vector $\vec{U} = [L_c\, L_1\, L_2\, L_3\, L_4]$. There exists an unknown and intricate relation (otherwise the inversion problem would be trivial to solve) between every component of $\vec{V}$ and the five components of $\vec{U}$. For the sake of generality we expressed

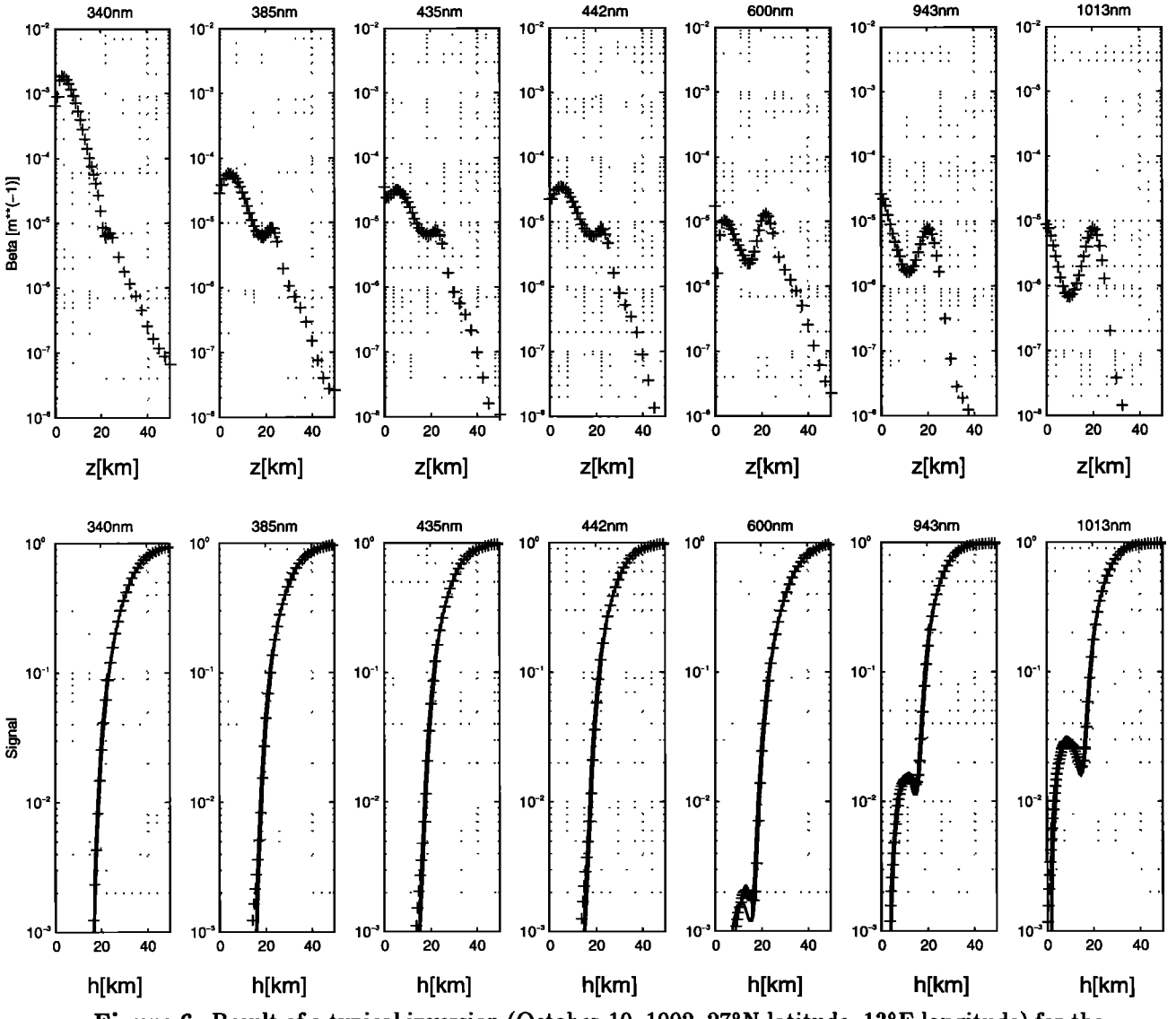

Figure 6. Result of a typical inversion (October 10, 1992, 27°N latitude, 13°E longitude) for the seven wavelengths used by ORA. (top): Retrieved total extinction profiles (1 m^{-1}= 1000 km^{-1}) versus altitude (km). (bottom): Measured signal (solid line) and computed signal (crosses) derived using the corresponding profiles above. Note the evolution of the aerosol layer signature as the wavelength increases.

this relation as a full cubic form of five variables (46 coefficients) as

$$V^{[i]} = \Theta^{[i]}(\overrightarrow{U}) \ \{i = 1, \ldots 5\} \qquad (24)$$

The matrix Θ has been determined by a linear least - squares fit over the whole synthetic signal data set. By using (24), it is then possible to predict the used parameters with moderate accuracy (standard deviation is 0.43 km on z_c and 0.32 km on c_3). This mapping can be used to compute a generic aerosol profile, which in turn, is added to the other extinction profiles (due to other constituents) to produce the $w(z)$ function in each channel.

The final flowchart for the spatial inversion scheme has been summarized in Figure 5, and its completion required about 10^9 flops for each occultation event (within seven usable channels).

7. Results and Conclusions

In Figure 6 we report the final solution obtained for a typical occultation. The mean $\xi = \sqrt{\chi^2/k_m}$ residual (i.e., the mean deviation between the measured transmission and the transmission obtained from the solution profile) was found to increase slightly with wavelength ($\xi \simeq 0.0010$ at $\lambda = 340$ nm to $\xi \simeq 0.0026$ at $\lambda = 1013$ nm). The value of ξ does not seem to be determined by the experimental noise ($\sim 10^{-4}$) but more probably by possible systematic errors in the description of the refraction processes, the discretization and interpolation schemes used for the Sun or the atmosphere and the NOPE method itself. At altitudes above 45 or 50 km, possible erratic profile behaviors can be observed which are cancellation effects between the $\overrightarrow{\alpha}$ coefficients (keeping in mind the very large dynamical range of the extinction coefficients). It is evident that the mapping strategy has given a somewhat more important weight to the inversion in the region of the aerosol layer because it became an important topic. On the other hand, the occultation method is limited at high altitudes because the attenuation is too weak, and at low altitudes because it is too strong (saturation), rendering the signal insensitive to the profile. A lower bound for the minimal meaningful signal would be 1 to 2×10^{-3}, while information can be extracted for $\beta(z)$ ranging between 10^{-5} and 10^{-1} km^{-1}.

A quick inspection of Figure 6 reveals that the reduced relative importance of the aerosol layer is reduced as the wavelength decreases. For $\lambda = 600$ nm the aerosol peak exhibits a shoulder due to the ozone contribution. It is the purpose of the spectral inversion to extract the constituent density number by using the related cross sections in all channels.

All the occultations measured by ORA between August 1992 and May 1993 have now been fully processed and stored. In the near future we will develop the spectral inversion algorithm in parallel with the investigation of directly exploitable channels (like $\lambda = 1013$ nm, almost exclusively sensitive to the aerosol) and their validation with respect to other experiments. A complete error analysis will also be performed.

The spatial inversion algorithm of ORA appears to be able to retrieve extinction profiles with a much better altitude resolution than one would have expected by considering the large field of view of the instrument. The method is numerically quite expensive but nevertheless offers some warranty for the obtained solution, which some heuristic schemes do not. The condition sine qua non for such an instrument being competitive with more sophisticated experiments is, of course, the recording of a quasi noiseless signal.

Acknowledgments. The authors wish to express their gratitude to Ian Burchell of the University of Oxford and Freddy Brouillard of the Université Catholique de Louvain for drawing their attention to the dilution effect. The mapping strategy was developed after fruitful discussions with J. Lenoble and C. Brogniez of the Université de Lille. This work was partly supported by the Fonds National de la Recherche Scientifique of the Belgian government under contract 1.5.207.95F.

References

Abramowitz, M., and I. A. Stegun, *Handbook of Mathematical Functions*, Dover, Mineola, N. Y., 1972.

Allen, C. W., *Astrophysical Quantities*, 3rd ed., Athlone , London, 1985.

Arijs, E., D. Nevejans, D. Fussen, P. Frederick, E. V. Ransbeek, F. W. Taylor, S. B. Calcutt, S. T. Werrett, C. L. Heppelwhite, T. M. Pritchard, I. Burchell, and C.D.Rodgers, The ORA occultation radiometer on EURECA, *Adv. Space Res.*, *16*, 833–836, 1995.

Born, M., and E. Wolf, *Principles of Optics*, Pergamon, Tarrytown, N. Y., 1993.

Brogniez, C., and J. Lenoble, Analysis of 5-year aerosol data from the Stratospheric Aerosol and Gas Experiment, *J. Geophys. Res.*, *96*, 15,479–15,497, 1991.

Calcutt, S. B., T. M. Pritchard, C. L. Heppelwhite, F. W. Taylor, S. T. Werret, E. A. Arijs, and D. Nevejans, A radiometer for the measurement of water vapour in the upper atmosphere from space, 1, Experiment concept and instrument description, *Appl. Opt.*, *32*, 6764–6776, 1993.

Chahine, M. T., A general relaxation method for inverse solution of the full radiative transfer equation, *J. Atmos. Sci.*, *29*, 741–747, 1972.

Edlen, B., The dispersion of standard air, *J. Opt. Soc. Am.*, *43*, 339–345, 1953.

Fussen, D., NOPE : A new inversion method for the total absorption profile retrieval of the ORA space experiment, in *Proceedings of the Second European Symposium on Satellite Remote Sensing*, vol. 2582-11, 80–87, SPIE, Bellingham, W., 1995.

Garriott, O. K., Visual observations from space, *J. Opt. Soc. Am.*, *69*, 1064–1068, 1979.

Kent, G. S., D. M. Winker, M. T. Osborn, and K. M. Skeens, A model for the separation of cloud and aerosol in SAGE II occultation data, *J. Geophys. Res.*, *98*, 20,725–20,735, 1993.

Lumpe, J. D., C. S. Chang, and D. J. Strickland, Atmospheric constituent density profiles from full disk solar occultation experiments, *J. Quant. Spectrosc. and Radiat. Transfer*, *46*, 483–506, 1991.

Mauldin L. E., III, N. H. Zaun, M. P. McCormick, J. H. Guy, and W. R. Vaughn, Stratospheric Aerosol and Gas Experiment II instrument: A functional description, *Opt. Eng.*, *24*, 307–312, 1985.

Press, W. H., S. A. Teukolsky, W. T. Vetterling, and B. P. Flannery, *Numerical Recipes in FORTRAN*, 2nd ed., Cambridge Univ. Press, New York, 1992.

Roble, R. G., and P. B. Hays, A technique for recovering the vertical number density profile of atmospheric gases from planetary occultation data, *Planet. Space Sci.*, *20*, 1727–1744, 1972.

Roche, A. E., J. B. Kumer, J. L. Mergenthaler, G. A. Ely, W. G. Uplinger, J. F. Potter, T. C. James, and L. W. Sterrit, The cryogenic limb array etalon spectrometer (CLAES) on UARS: Experiment description and performance, *J. Geophys. Res.*, *98*, 10,763–10,775, 1993.

Rodgers, C. D., Retrieval of atmospheric temperature and composition from remote measurements of thermal radiation, *Rev. Geophys.*, *14*, 609–624, 1976.

Russell, J. M., III , L. L. Gordley, J. H. Park, S. R. Drayson, W. D. Hesketh, R. J. Cicerone, A. F. Tuck, J. E. Frederick, J. E. Harries, and P. J. Crutzen, The Halogen Occultation Experiment, *J. Geophys. Res.*, *98*, 10, 777–10,797, 1993.

Twomey, S., Comparison of constrained linear inversion and an iterative nonlinear algorithm applied to the indirect estimation of particule size distributions, *J. Comput. Phys.*, *18*, 188–200, 1975.

E. Arijs, C. Bingen, D. Fussen, F. Leclere and D. Nevejans, Belgian Institute for Space Aeronomy (IASB-BIRA), 3, avenue Circulaire, B-1180 Bruxelles, Belgium (e-mail: Didier.Fussen@oma.be)

(Received December 20, 1995; revised September 18, 1996; accepted September 18, 1996)